Journal of Physical Science, Vol. 33(2), 125–138, 2022

Performance and Analysis of a Designed Magnetic Lens for Microscopic Applications

Emad H. Ahmed* and Adnan K. Hasan

Department of Physics, Collage of Science, Mustansiriyah University, Baghdad, Iraq

*Corresponding author: emadhameed321@uomustansiriyah.edu.iq, khalidadnan729@gmail.com

Published online: 25 August 2022

To cite this article: Ahmed, E. H. & Hasan, A. K. (2022). Performance and analysis of a designed magnetic lens for microscopic applications. *J. Phys. Sci.*, 33(2), 125–138. https://doi.org/10.21315/jps2022.33.2.8

To link to this article: https://doi.org/10.21315/jps2022.33.2.8

ABSTRACT: *The magnetic lens (magnetic field lens) uses a magnetic field rather than an equipotential plane. This work presents a modelling of the design of a focused magnetic lens. Its main purpose is to reveal the possibility of this lens to eliminate aberrations and to determine the extent of its potential to be included in the design of electron microscopes and electron beam melting systems. This work was accomplished by using COMSOL Multiphysics simulation software. The magnetic lens was tested to determine the possibility of its inclusion in electron microscopes by changing the bore radius from 1 to 4 step by step. The proposed mathematical model was proven as an excellent tool in electron optics.*

Keywords: magnetic lens, COMSOL Multiphysics, aberration, electron optics

1. INTRODUCTION

Electron optics is a branch of charged particle optics science. The trajectories of charged particles are easily understood and directed through this science in accordance with the requirements of different applications, such as electron beam melting (EBM), ion beam deposition and electron microscopy.[1–3] Optical systems are mostly used to guide these energetic particles. The origin charged particle optics dates back to the first quarter of the 20th century when it was discovered that magnetic and electric fields can be used as lenses for electron imaging. The principal idea of electron optics is based

© Penerbit Universiti Sains Malaysia, 2022. This work is licensed under the terms of the Creative Commons Attribution (CC BY) (http://creativecommons.org/licenses/by/4.0/).

on two major revelations made in 1925 by de Broglie and in 1927 by Busch.[4] The Lorentz force (F) equal to $q(v\ B + E)$ is the force acting on a single particle.[5] One of the most distinguishing characteristics of Lorentz force magnetic component is that it is perpendicular to the electrons' velocity and the magnetic field. The aberration conditions in electron optics are not as easily quantifiable or descriptive of the device through which the electrons have passed as they are in conventional optics.[6] In electron optics, a cylindrical lens formed from a solenoid looped around the optical axis is known as a magnetic focus lens.[7] The electrons curve in a circular motion towards the optical axis when the field is aligned with the optical axis to eliminate these aberrations.[8] The coil produces a magnetic field that curves outwards from the coil centre but is parallel to the optical axis within the coil.[9] When an electron enters the coil at a velocity that is not totally parallel to the magnetic field, it is deflected back towards the optical axis.[10] This criterion is easily satisfied because the magnetic field changes direction along the optical axis.[11] Only electrons travelling along and totally parallel to the optical axis are not subjected to a focusing force.[12] Magnetic lenses are used in a variety of scientific and commercial applications, including optics, transmission electron microscopy (TEM), scanning electron microscopy, accelerators and a variety of electron beams emitted focusing devices.[13–15] A pole piece, electromagnetic coil, and magnetic yoke formed the traditional TEM apparatus.[16] As shown in Figure 1, the magnetic field created around the electromagnetic coils is directed to concentrate in an area near the pole piece.[9] The effect of current density and lens size on the design of iron-free magnetic lenses was investigated in a few previous studies. A magnetic field was observed for varying current density values.[17] Other investigations explored the single and double pole magnetic lens objective features at different pole shapes.[18,19] Patil et al. introduced a concept of the magnetic lens, which was composed of high permeability ceramic ferrites to enhance the output performance of magneto-mechano-electric (MME) energy generator.[20] The magnetic lens was found to enhance the output voltage of MME generator by concentrating the weak magnetic flux originating from the magnetic field sources on the magnetic constituents in MME structure. The feasibility of using a magnetic lens as a magnetic flux condenser was first evaluated using finite element analysis. The simulation results were then experimentally verified by harvesting the weak fields originating from the Helmholtz coil. The MME generator with a magnetic lens composed of four ferrites exhibited enhancement of 288% and 125% over that of MME generator without a lens and with a lens composed of one ferrite, respectively. The main purpose of this work is to reveal the possibility of this lens to eliminate aberrations and to determine the extent of its potential to be included in the design of electron microscopes and electron beam melting systems.

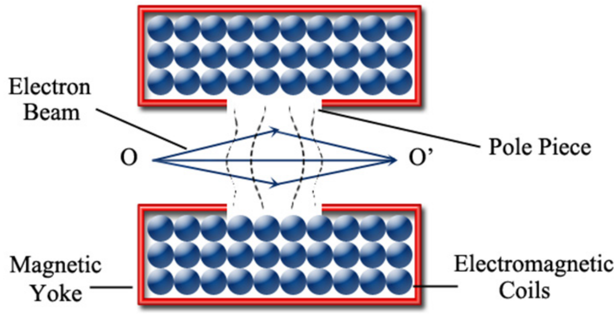

Figure 1: Schematic of the forming equipment of a magnetic focusing lens.

2. MATERIALS AND METHODS

2.1 Lens Design

The model is defined in a vacuum cylinder that limits the level of the magnetic field and the trajectory of the particle.[21] The cylinder has a height of 1 m and a radius of 10 cm, which corresponds to the standards commonly used in EBM systems. The cylindrical boundary is designed as a perfect magnetic insulator, which indicates that no magnetic field is found in the normal direction to the boundary surface. Electrons are initiated at the bottom centre of the vacuum cylinder with a velocity corresponding to a kinetic energy of 60 keV in the positive z direction. The electrons then pass through a magnetic lens that focuses, deflects and corrects the electron beam. Electrons continue to bypass the magnetic lens to the top of the vacuum cylinder. The repulsion of the space charge is the dominant force on the electrons in this region because the magnitude of the magnetic field decreases when the electrons move away from the magnetic coil.[22] Figure 2 shows the magnetic field size of the magnetic focus lens, gradient from blue to red and a red streamlined direction of this field. The deflection lens where the deflection field is completely aligned with one of the poles in a quadrupole coil is plotted in Figure 3(a). The deflection lens where the deflection field is aligned to the angle $\pi/4$ in accordance with the pole axes is shown in Figure 3(b).

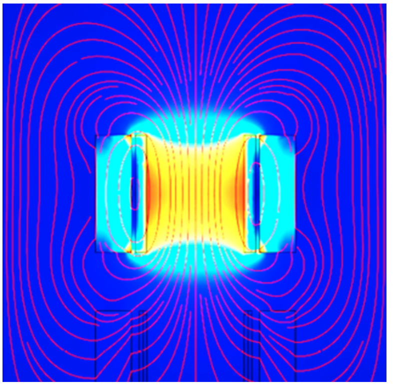

Figure 2: Magnetic field pattern is caused by the focusing coil being in an axis parallel to the optical axis.

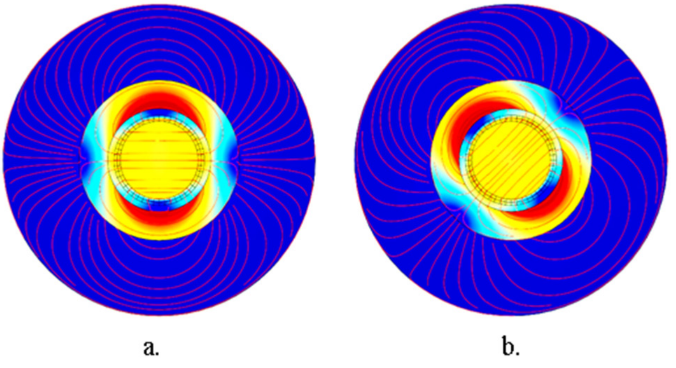

Figure 3: Deflection field alignment: (a) wholly aligned with one of the poles in a quadrupole coil and (b) the deflection is aligned to the angle π/4 in accordance with the pole axes.

2.2 Mathematical Determinations

2.2.1 Magnetic scalar potential determination

The pole piece profile of magnetic lens is scalar potential, which was discovered to be an important duty. The axial magnetically scalar potential distribution $V(z)$, with an optical axis of the magnetic lens, is expressed on the basis of the current study of synthesis technique.[23]

$$V(z) = \frac{1}{2}\left[(V_1 + V_2) + (V_1 - V_2)\tanh\left(\frac{1.32z}{R}\right)\right] \tag{1}$$

2.3 Calculation of Magnetic Field Distribution

The axial magnetic field distribution along the lens region can be derived by using a differential equation and shifting it to reduced Maxwell's equation $B_z = -\mu \dfrac{dv_z}{dz}$.[23] Equation (1) then becomes:

$$B_z(z) = \mu_o\left(\frac{V_2 - V_1}{2}\right)\left(\frac{1.32}{R}\right)\operatorname{sech}^2\left(\frac{1.32z}{R}\right) \tag{2}$$

Equation (2) can then be used to assign the interplanetary magnetic field distribution $Bz(z)$ along the optical axis $zs \le z \le zf$ when the magnetic field (MF) is determined. The field in Equation (2) represents a field of projector lens in the electron microscope. The second derivative of the potential distribution with respect to the axial coordinate z is expressed as

$$V''(z) = -(V_2 - V_1)\left(\frac{1.32}{R}\right)^2\tanh\left(\frac{1.32z}{R}\right)\operatorname{sech}^2\left(\frac{1.32z}{R}\right) \tag{3}$$

2.4 Pole Piece Profile

The state of the pole piece that will generate the ideal region of study can be resolved by using the scientific arrangement of Laplace condition. The electrostatic or attractive scalar potential V (R_P, z) for pivotally symmetric frameworks can be calculated from the hub appropriation of a similar potential $V(z)$ by the accompanying arrangement extension.[24]

$$V(R_p, z) = \sum_{k=0}^{\infty}\frac{(-1)^k}{(k!)^2}\left(\frac{R_p}{2}\right)^{2k}\frac{d^{2k}V(z)}{dz^{2k}} \tag{4}$$

Where R_p is the radial height of the equipotential surface. The model that has been introduced for the first time by Garche (2009) for electrostatic lenses is used to determine the pole piece profile.[10] The equipotential field (i.e. the pole piece) by taking the first two conditions of Equation (5) is expressed as:

$$R_P(z) = 2\sqrt{\left[\frac{V(z) - V_P}{V''(z)}\right]} \tag{5}$$

where V_P is the potential value in the surface of the pole piece, which corresponds to half the excitation of the lens (*NI*) in the case of a symmetrical lens at the field connections, and *Vz* is the second derivative of the scalar magnetic potential with respect to the *z* coordinate.

3. RESULTS

A quadrupole coil model was used to reduce the sinusoidal distribution geometry to three circular coils along with the cylinder as shown in Figure 4(a). Each pole consisted of three coils having an angular width of π/2.[25] This condition indicates that the quadrupole needs to consist of three separated shells to be fitted with the quadrupole.[26] The superposition model assumption is valid if the distance between the coils is shorter than the distance to the beams (as shown in Figure 4[b]).

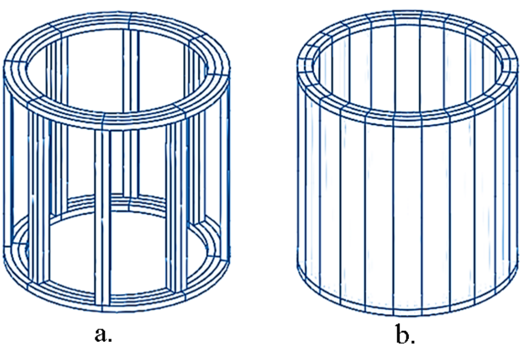

Figure 4: (a) Renders of the bar model used to simulate a quadrupole coil and (b) Render of a coil based on the superposition model divided into 24 angular segments.

One of the advantages of superposition models is the possibility of designing coils with many different poles, each with different currents, within the same geometry as obtained from this model in Figure 5.[27] This advantage gives users the ability to experiment with different coil, pole or current configurations by changing the individual currents accordingly. As shown in Figure 5(a), the quadrupole fields were created by orienting the opposing dipole fields on the opposite sides of the optical axis as opposed to the dipoles.[28] This condition indicates that the fields are bent outwards and disappear from the centre until the diffraction theory stops. A circular beam was formed by charged particles focused on the first axis and defocused from the second axis to eliminate and correct the twofold astigmatism.[29] In the other two cases in Figures 5b and 5c, the hexadecapole and octupole stigmators consist of alternating fields. The difference depends on the symmetry, where the octupole is fourfold, and its task is correcting the four-symmetric aberrations each in accordance with its condition.[30] If an octapolar is used with a quadrupole, then eliminating the spherical aberrations on x-axes and y-axes will be easy in addition to correcting the fourfold astigmatism in the middle. The hexadecapole has a threefold symmetry that is used to firstly reduce third-order spherical aberration and then eliminate threefold astigmatism in the most complicated electron microscopes.[31]

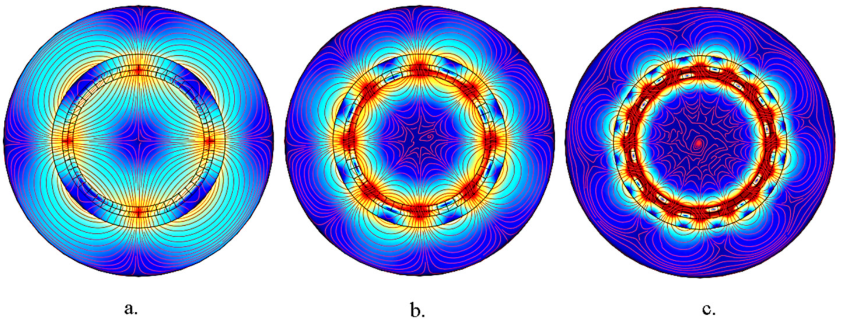

Figure 5: Designed coils with many different poles; (a) quadrupole $n = 4$, (b) octupole $n = 8$ and (c) hexadecapole $n = 16$.

The deflection and focus set up of magnetomotive force (MMF) represented by the current times the number of turns as a function of deflecting angle is illustrated in Figure 6. The beam entered through the model at the origin point traverses the focusing lens at 220 mm and the deflecting lens at 310 mm and stops at 1000 mm. The deflection field is emanated from a single dipole in the first case, where the angle = 90° at a deflection current = I. In the second case, the angle is 45° with the deflection of two perpendicular dipoles to each other with the value of currents = Ix, Iy. A procedure was taken to normalise the values of the currents by calculating the square root of the sum of the squares of the currents on each axis. Figure 7 shows how the influence of space charge and lens size can be explored by looking at how the beams' behaviour varies as they are focusing closer to the lens. The beam size converges with the increase in MMF.

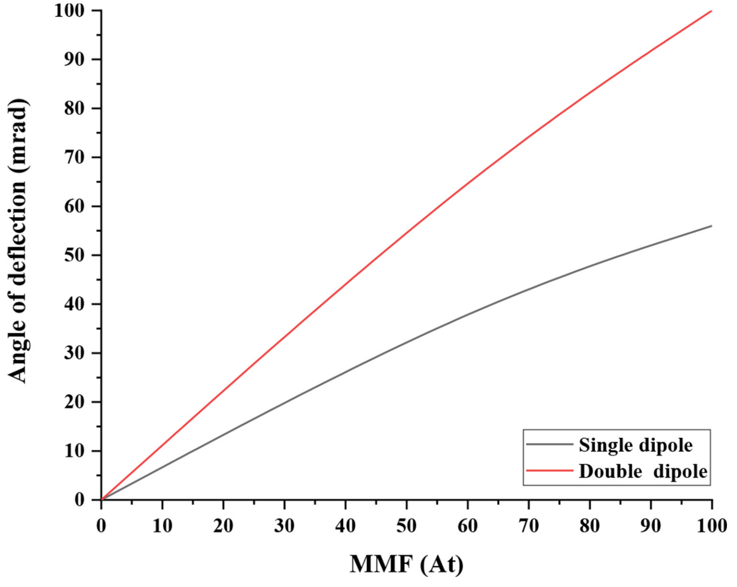

Figure 6: Angles of deflection for a single and a double dipole based on current and number of turns.

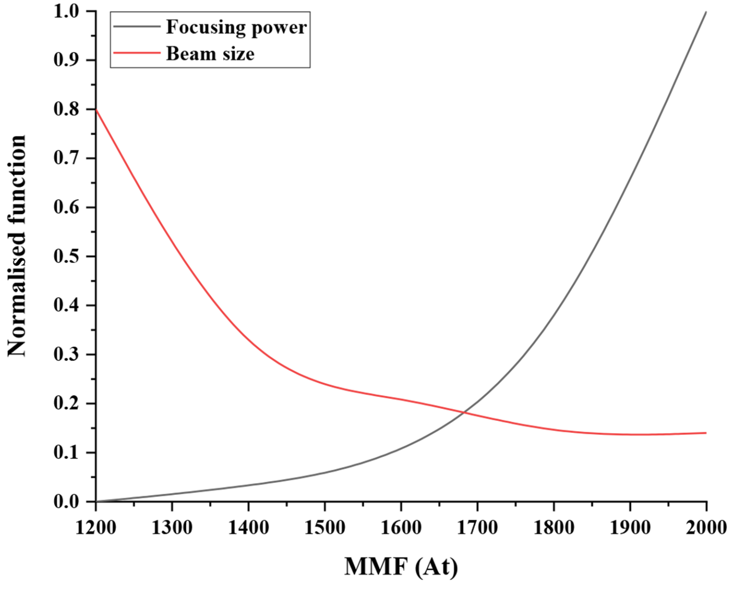

Figure 7: Normalised 24 varied setting of I and n of a magnetic focus of lens focusing power and beam size.

In this work, this magnetic lens design was tested to determine the possibility of reinstalling it with projector devices in electron microscopes (the data are listed in Table 1).[32] In accordance with Equation 1, the most important variable, the bore radius affects the distribution of fields and numerical potentials with magnetic properties. The same applies to the projector of magnetic double symmetrical pole piece lenses. Thus, mag-scalar and mag-field may have the best distribution due to the influence of variable values that contribute to improving their indications.

Table 1: Projector attributes and half width W (mm) for various values of bore radius

R	$F_{p\,min}$	$NI/\sqrt{V_r}$	Dr at $NI/\sqrt{V_r}$	Ds at $NI/\sqrt{V_r}$	W
1	0.76	14.31	0.37	2.01	1.34
2	1.52	14.31	0.07	0.51	2.27
3	2.37	14.31	0.03	0.22	4.01
4	3.03	14.31	0.02	0.12	5.34

Note: Ds is the spiral distortion coefficient and Dr is the radial distortion coefficient.

In Figure 8, the variation of the axial flux density, symbolised by Bz, is explained with different values of the bore radius, symbolised by R as 1 mm, 2 mm, 3 mm, 4 mm and 5 mm. The field is distributed in a narrow beam when the values of R are minimal and vice versa. A symmetrical gradient distribution of the potential function is observed around the mid-plane when the values of R are increased, as plotted in Figure 9. This finding is supported by the Ampere critical law theorem. Accordingly, half the width (w) of the field distribution is directly proportional to R, where it increases with increasing radius of the lens cavity. The maximum value of the field distribution decreases with the increase in R, as shown in Figure 10.

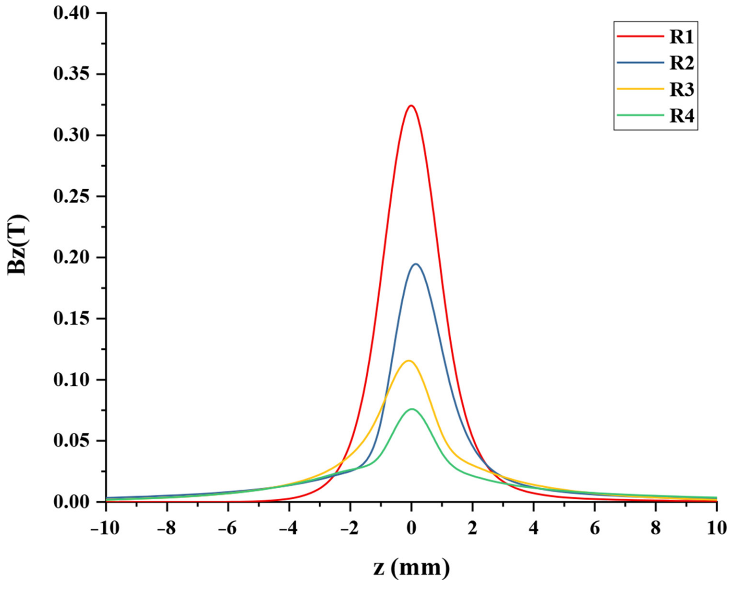

Figure 8: Axial magnetic field distribution B_z for many values of R.

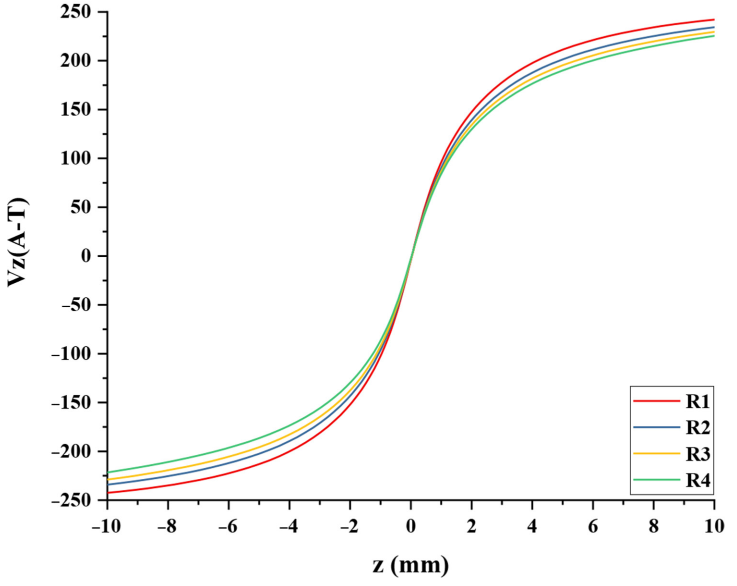

Figure 9: Distribution of the axial magnetic scalar potential for many values of R.

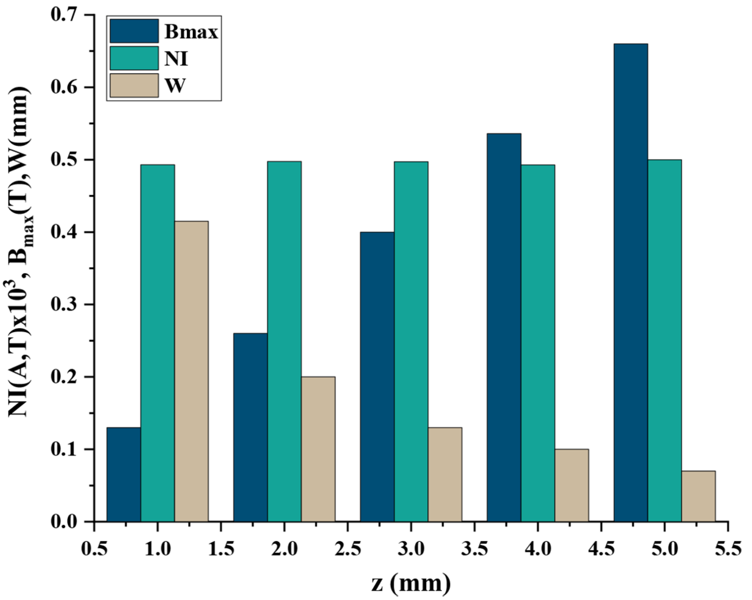

Figure 10: Variation of *W*, *Bmax* and *NI* with bore radius *R*.

4. CONCLUSIONS

In electron microscopy, a major portion of the existing literature review was devoted to aberration measurements and corrections. This condition was primarily because that no other aspect of electron optics has achieved the same level of advancement as aberration correction. A number of issues must be resolved before the insights gained by our model can be applied in a practical electron optic machine. This research showed that mitigating aberrations without access to measurements of the actual beam profile in the system will be extremely difficult. This form of assessment can be used to test and enhance models, and as part of a feedback-based correction system. The present work used the mathematical model of the scalar potential for the first time and was demonstrated as an excellent tool in electron and ion optics by the synthesis procedure, where the projector focal properties of this model for double pole piece magnetic lenses will be investigated in depth. This methodology can be successfully incorporated in future work to advance the succeeding appealing focal points.

5. ACKNOWLEDGEMENTS

The authors thank Mustansiriyah University, Baghdad, Iraq for supporting this work.

6. REFERENCES

1. Körner, C. (2016). Additive manufacturing of metallic components by selective electron beam melting: A review. *Int. Mater. Rev.*, 61(5), 361–377. https://doi.org/10.1080/09506608.2016.1176289
2. Vats, N. et al. (2018). Electron microscopy of polyoxometalate ions on graphene by electrospray ion beam deposition. *Nanoscale*, 10(10), 4952–4961. https://doi.org/10.1039/c8nr00402a
3. Egerton, R. F. (2016). *Physical principles of electron microscopy: An introduction to TEM, SEM, and AEM*, 2nd ed. New York: Springer International Publishing.
4. Wilson, E. J. N. (1977). Charged particle beams. *Nature*, 270(5639), 764–764. https://doi.org/10.1038/270764b0
5. Rose, H. (2009). *Geometrical charged-particle optics*. Berlin/Heidelberg: Springer.
6. Septier, A. (2017). The struggle to overcome spherical aberration in electron optics. *Adv. Imag. Electron Phys.*, 202, 75–147. https://doi.org/10.1016/bs.aiep.2017.06.001
7. Namba, S. et al. (2019). Experimental realization of a hybrid trapped field magnet lens using a GdBaCuO magnetic lens and MgB2 bulk cylinder. *Supercond. Sci. Technol.*, 32(12), 1–12. https://doi.org/10.1088/1361-6668/ab5048
8. Egerton, R. (2005). Chapter 2 electron optics. In R. Egerton (Eds.). *Physical principles of electron microscopy*, 2nd ed. Cham, Switzerland: Springer, vol. XII, 202.
9. Abd Alghane, B. & Ahmad, A. (2021). Design of symmetric magnetic lenses with optimum operational conditions. *Al-Nahrain J. Sci.*, 24(1), 30–38. https://doi.org/10.22401/anjs.24.1.06
10. Garche, J. (2009). *Encyclopedia of electrochemical power sources*. Amsterdam: Elsevier.
11. Melnikov, A. A. & Potapkin, O. D. (2008). On electron movement through magnetic electron lens. *Phys. Procedia*, 1(1), 207–215. https://doi.org/10.1016/j.phpro.2008.07.098
12. Franken, L. E. et al. (2020). A technical introduction to transmission electron microscopy for soft-matter: Imaging, possibilities, choices, and technical developments. *Small*, 16(14), 1906198. https://doi.org/10.1002/smll.201906198

13. Shamuilov, G. et al. (2021). Optical magnetic lens: Towards actively tunable terahertz optics. *Nanoscale*, 13(1), 108–116. https://doi.org/10.1039/d0nr06198k
14. Goodhew, P. J. (2011). General introduction to transmission electron microscopy TEM. In P. J. Goodhew (Eds.). *Aberration-corrected analytical transmission electron microscopy*. New Jersey: John Wiley and Sons, 1–19. https://doi.org/10.1002/9781119978848.ch1
15. Ogawa, T. et al. (2022). A novel monochromator with offset cylindrical lenses and its application to a low-voltage scanning electron microscope. *Microsc. Microanal.*, 28(2), 412–424. https://doi.org/10.1017/S1431927622000150
16. Montgomery R. P. E. (2008). *Fundamentals of HVAC control systems (IP)*. Amsterdam: Elsevier Inc.
17. Alamir, A. S. A. (2003). A study on effect of current density on magnetic lenses. *Optik*, 114(2), 85–88. https://doi.org/10.1078/0030-4026-00226
18. Sultan, S. et al. (2020). Effect of pole face thickness on magnetization of the single-pole magnetic lens. *Rafidain J. Sci.*, 29(4), 44–52. https://doi.org/10.33899/rjs.2020.167315
19. Baba, N. (1978). Magnetic einzel lens satisfying anastigmatic and achromatic conditions. *Proceedings, Annu. Meet. Electron Microsc. Soc. Am.*, 36(1), 26–27.
20. Patil, D. R. et al. (2022). Boosting the performance of magneto-mechano-electric energy generator using magnetic lens. *Sens. Actuators A Phys.*, 338, 113451. https://doi.org/10.1016/j.sna.2022.113451
21. Tien, C. & Ramarao, B. V. (2007). Trajectory analysis of particle deposition. In *Granular filtration of aerosols and hydrosols*. Amsterdam: Elsevier, 169–211.
22. Tien, C. & Ramarao, B. V. (2007). *Granular filtration of aerosols and hydrosols*. Amsterdam: Elsevier Ltd.
23. Wilcox, A. (1988). Computer-aided design in magnetics. *Comput. Meth. Appl. Mech. Eng.*, 66(2), 252–253. https://doi.org/10.1016/0045-7825(88)90080-1
24. Cheng, M. & Tang, T. (2001). Curvilinear-axis focusing and aberration theory of wide electron beams for combined electrostatic-immersion magnetic lens systems. *Optik*, 112(6), 259–267. https://doi.org/10.1078/0030-4026-00053
25. Schachinger, T. et al. (2021). Experimental realization of a π/2 vortex mode converter for electrons using a spherical aberration corrector. *Ultramicroscopy*, 229, 113340. https://doi.org/10.1016/j.ultramic.2021.113340
26. Rebrov, V. A. et al. (2007). The new design of magnetic quadrupole lens doublet manufactured from a single piece. *Nucl. Instruments Methods Phys. Res. Sect. B Beam Interact. with Mater. Atoms*, 260(1), 34–38. https://doi.org/10.1016/j.nimb.2007.01.275
27. Brydson, R. (2011). *Aberration-corrected analytical transmission electron microscopy*. New Jersey: John Wiley and Sons.
28. Kolinko, S. V. et al. (2013). Precise centering and field characterization of magnetic quadrupole lenses. *Nucl. Instruments Methods Phys. Res. Sect. A Accel. Spectrometers, Detect. Assoc. Equip.*, 700, 70–74. https://doi.org/10.1016/j.nima.2012.10.072
29. Hetherington, C. (2004). Aberration correction for TEM. *Mater. Today*, 7(12), 50–55. https://doi.org/10.1016/S1369-7021(04)00571-1

30. Kuzmiak, M. et al. (1988). Focusing and decreasing the effective emittance of hollow charge particle beams by octupole magnetic lenses. *Czechoslov. J. Phys.*, 38(3), 275–282. https://doi.org/10.1007/BF01597653
31. Chaustowski, R. R. et al. (2007). Magnetic hexapole lens focusing of a metastable helium atomic beam for UV-free lithography. *Appl. Phys. B Lasers Opt.*, 86(3), 491–496. https://doi.org/10.1007/s00340-006-2497-2
32. Rose, H. H. (2008). Optics of high-performance electron microscopes. *Sci. Technol. Adv. Mater.*, 9(1), 014107. https://doi.org/10.1088/0031-8949/9/1/014107